DALTON

# Chromium luminescence as a probe of site effects in the alum lattice

**Robert S. Armstrong, Andrew J. Berry, Bradley D. Cole and Kerry W. Nugent**

*School of Chemistry, University of Sydney, NSW 2006, Australia*

The $^2E_g \longrightarrow {}^4A_{2g}$ transition of chromium(III) doped in $CsM^{III}(XO_4)_2 \cdot 12H_2O$ ($M^{III}$ = Cr, Al, Ga, In, Co, Rh or Ir, X = S; $M^{III}$ = Cr, Al, Ga, In or Rh, X = Se) has been measured. The emission spectra are interpreted in terms of the α and β alum structures. The energy and splitting of the electronic origin are determined by the nature and magnitude of a trigonal field. The trigonality is attributed to a combination of polarisation effects arising from groups oriented along the three-fold axis, and π overlap between the co-ordinated water lone pair and chromium $t_{2g}$ orbitals. The polarisation effect is strongly dependent on the counter ion and chromium site size. The degree of π overlap is determined by the water co-ordination geometry, defined by both electronic stabilisation factors and hydrogen-bonding interactions with the host lattice. π Overlap is favoured by the trigonal-planar water co-ordination to chromium in the β lattice. This results in a large origin splitting and low transition energy relative to the α alums where π overlap is reduced by trigonal-pyramidal water co-ordination. Variations in the emission, within an alum class, are the result of the polarisation strength of the counter ion, and distortions to the chromium co-ordination environment imposed by the host lattice.

The caesium alums $CsM^{III}(XO_4)_2 \cdot 12H_2O$ (X = S or Se) crystallise in the cubic space group *Pa*3, and are structurally stable to liquid-helium temperatures. The alum structure can accommodate a wide range of trivalent hexaaqua cations with little change to the lattice, making it well suited to a comparative study of the structure and bonding of trivalent metal ions in a fixed environment. The caesium alums occur in two structural classes α and β.[1–3] The classes are distinguished by crystal morphology, caesium co-ordination, and the mode of water co-ordination to the trivalent ion. The type of alum is usually dependent on the size of the monovalent cation relative to the counter ion or unit-cell size. For caesium in a sulfate lattice the caesium cation is usually accommodated by cubo-octahedral co-ordination, characterising the β form. The six caesium water molecules lie in a plane perpendicular to the three-fold axis, while six oxygens from two sulfate groups are positioned both above and below this plane. In a selenate alum the smaller relative size of the caesium produces icosahedral co-ordination resulting from a puckering of the plane of water molecules. This geometry is characteristic of the α modification (Fig. 1).

The alum lattice is characterised by strong hydrogen bonds that are approximately linear. The waters co-ordinated to the trivalent cation are hydrogen bonded to one sulfate/selenate oxygen and one oxygen of a water molecule co-ordinated to caesium (Fig. 1). The O–H · · · O angle has been determined by neutron diffraction to be 174–179° for the chromium,[5] iron,[4] and ruthenium[6] sulfate alums and for the iron selenate alum.[4] To satisfy the hydrogen-bonding linearity constraint the orientation of the waters co-ordinated to the trivalent cation varies according to the caesium co-ordination. In the β case trigonal-planar co-ordination of the water oxygen is observed, with a twist of the plane of the water molecule away from the molecular axes (Fig. 2). For the α alums the waters adopt a trigonal-pyramidal geometry, reflected by a tilt in the plane away from the $M^{III}$–O bond vector. This occurs in conjunction with a tilt of the $M^{III}O_6$ octahedron from the crystal axes. A large octahedron tilt necessitates a smaller tilt of the water molecules. It is also possible for the trivalent cation to determine the alum structure. In the case of $(t_{2g})^6$ metal ions, β-type water co-ordination is electronically unfavourable due to π overlap between the oxygen lone pair and fully occupied metal $t_{2g}$ orbitals. This forces α water co-ordination to the trivalent metal and imposes icosahedral caesium co-ordination through the hydrogen bonding. As a result the caesium sulfate alums of cobalt, rhodium and iridium adopt the α structural form.

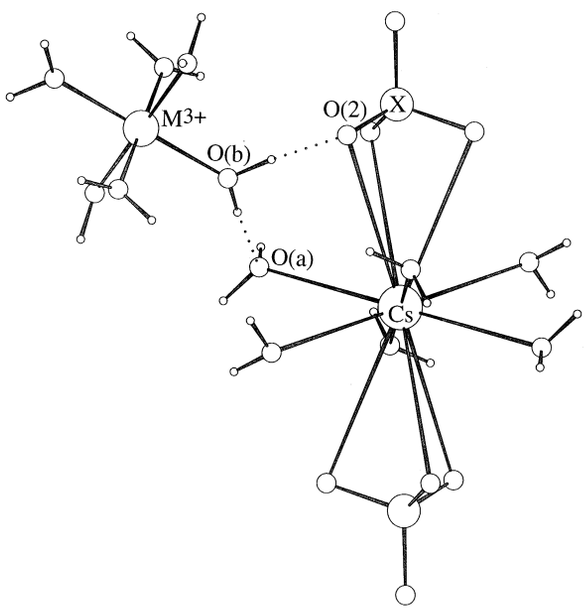


**Fig. 1** Caesium icosahedral co-ordination in the α alums. Hydrogen bonding to a water molecule co-ordinated to the trivalent cation is shown. The figure is drawn using neutron diffraction data from ref. 4

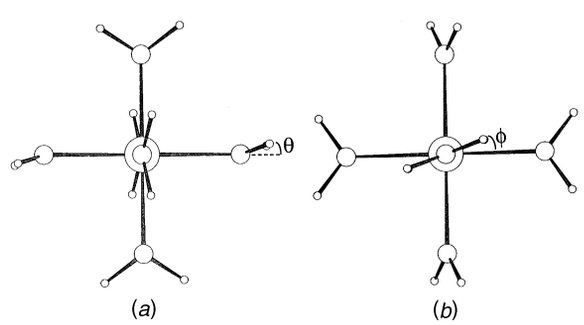


**Fig. 2** Stereochemistry of water co-ordination to the trivalent cation showing (*a*) the angle of tilt, θ, in the α alums and (*b*) the angle of twist, φ, in the β alums; drawn using neutron diffraction data from ref. 4

The $^2E_g \longrightarrow {}^4A_{2g}$ transition of chromium(III) has been exten-

sively studied,[7–14] and low-temperature absorption spectra of chromium(III) doped into a variety of alum lattices have previously been reported.[15] An analysis of the absorption and emission spectra of $CsCr(SO_4)_2 \cdot 12H_2O$ has also been undertaken in terms of the trigonal-field splitting of the $^2E$ state.[16] The $^2E_g \longrightarrow {}^4A_{2g}$ transition in the alum lattice has been recorded for dopant levels below 0.5 ppm.[17] The sensitivity of detection indicates the use of chromium as a probe of lattice structure. Using the recently refined structural information[4–6] and our new spectroscopic results for the caesium alums, the differences in emission for α and β alums can now be explained. Further, our understanding of the effect of structural variations on the emission will allow interpretation of site effects, illustrating how an impurity responds to meet the requirements imposed by its environment.

## Experimental

Sulfate alums of Cr,[18] Al,[19] Ga,[1] In,[1] Co,[20] Rh[21] and Ir,[3] and selenate alums of Cr,[2] Al,[2] Ga,[2] In[2] and Rh,[21] were prepared by standard methods. Doped alums were prepared by dissolving a stoichiometric amount of the chromium and host lattice alums in the appropriate 1 mol $dm^{-3}$ acid, to produce crystals with a nominal dopant level of 1% by site. Single crystals were mounted in an Oxford Instruments CF 1204 continuous-flow cryostat. Excitation was with the 476.49 nm line of a Spectra Physics 2020-05 argon-ion laser. Luminescence was collected perpendicular to the excitation and focused onto the slits of a Jobin-Yvon U1000 double monochromator. The signal from a RC 31034 photomultiplier tube was processed by a Princeton Applied Research 1120 discriminator/preamplifier and the spectrum compiled by a Jobin-Yvon spectra link acquisition board under computer control. Transition energies were determined relative to the laser line, with $\nu_1(XO_4^{2-})$ in the Raman spectrum providing an internal energy calibration.

## Results and Discussion

The emission spectra of chromium in a variety of alum host lattices were recorded at 6 K. Two distinct emission types were observed corresponding to alum structure. For the α alums an intense doublet of variable separation was observed at around 14 950 $cm^{-1}$ (Fig. 3). For the β alums there is only a single intense line, shifted by around 500 $cm^{-1}$ to lower energy compared with the α alums, although at 80 K a band was observed at 125 $cm^{-1}$ to higher energy. This is in close agreement with earlier work where a transition shifted from the origin by 120 $cm^{-1}$ was observed in absorption but not in emission.[16] These lines, and the α doublet, are assigned to the Boltzman-populated split components of the 0–0 $^2E_g \longrightarrow {}^4A_{2g}$ electronic origin transition. Table 1 gives the origin splitting, Δ, and mean origin energy, *E*.

To lower energy is an extensive and complicated vibrational structure (Fig. 4). Assignment of the major features was aided by the use of isotope-enriched chromium alums ($^{50}Cr$, $^{53}Cr$), deuteriated samples, and comparison with existing infrared and Raman data.[20–23] The structure is associated with normal modes of $[Cr(H_2O)_6]^{3+}$, and also modes of the caesium cation, the counter ion, and lattice, coupled to the emitting species by hydrogen bonding. A complete vibrational analysis was not attempted. Vibronic energies are similar to vibrational energies previously reported, although the infrared and Raman-inactive $\nu_6[Cr(H_2O)_6^{3+}]$ was identified at 227 $cm^{-1}$ for the chromium sulfate, and 218 $cm^{-1}$ for the chromium selenate alum.

The most intense vibronic transition is the ungerade $\nu_3[Cr(H_2O)_6^{3+}]$. The chromium movement associated with the antisymmetric stretch allowed confident assignment of this mode based on the $^{50}Cr$ and $^{53}Cr$ spectra. The band is also sharp, allowing accurate determination of variations in $\nu_3$ energy with host lattice. The $\nu_1$ symmetric stretch is expected to

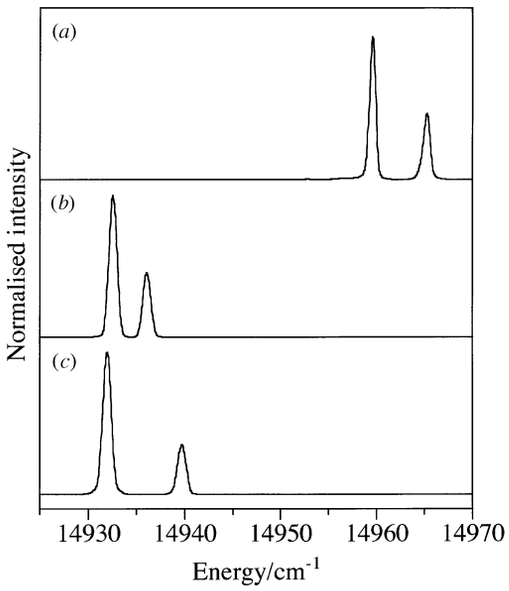


**Fig. 3** The split components of the $^2E_g \longrightarrow {}^4A_{2g}$ origin transition of $Cr^{3+}$ doped into the α alums (*a*) $CsRh(SO_4)_2 \cdot 12H_2O$, (*b*) $CsRh(SeO_4)_2 \cdot 12H_2O$, and (*c*) $CsIn(SeO_4)_2 \cdot 12H_2O$

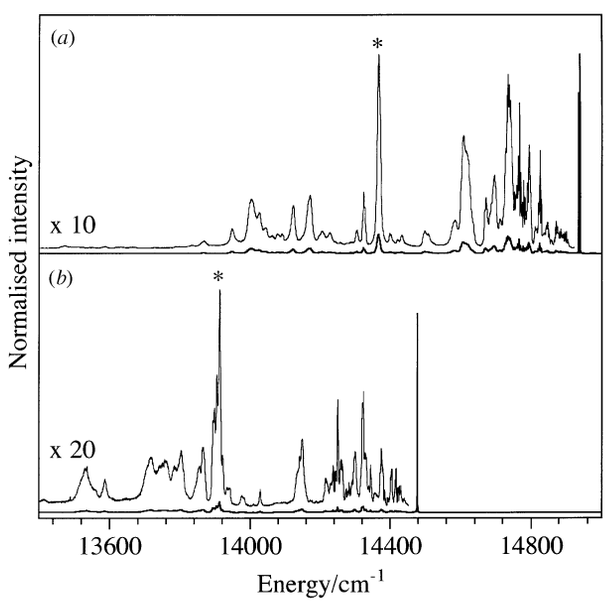


**Fig. 4** Vibrational structure associated with the $^2E_g \longrightarrow {}^4A_{2g}$ transition of $Cr^{3+}$ in (*a*) $CsCr(SeO_4)_2 \cdot 12H_2O$ and (*b*) $CsCr(SO_4)_2 \cdot 12H_2O$. * The asterisked peaks are assigned to $\nu_3[Cr(H_2O)_6^{3+}]$

be a more sensitive probe of site effects, but is both weak and broad in the emission. For both the sulfate and selenate alums the vibrational energy decreases with increasing site size in the series aluminium, gallium, indium (Table 1). The $\nu_3$ energy in $CsRh(SO_4)_2 \cdot 12H_2O$ is high, reflecting a unit-cell size smaller than the aluminium alum and a site size {defined by metal to hydrogen-bonding oxygen distances or the Wigner–Seitz cell volume[24] about $[M(H_2O)_6]^{3+}$} smaller than for the chromium alum. The α sulfate vibrational energies vary little; the reason for this is not clear.

The splitting of the electronic origin in the $^2E_g \longrightarrow {}^4A_{2g}$ emission of chromium(III) is well known from the R lines of ruby.[25] In this case the $CrO_6$ octahedron is trigonally distorted. In the alums the $CrO_6$ framework is approximately octahedral. The trigonal, $S_6$, site symmetry in both alum structures is a consequence of the twists (φ) and tilts (θ) of the co-ordinated water molecules (Fig. 2). The lowering of symmetry to $S_6$ does not in itself split the $^2E$ state. Instead the splitting derives from

**Table 1** The chromium site and $^2E_g \longrightarrow {}^4A_{2g}$ transition energies: *a* is the unit-cell dimension, M–O(a) and M–O(2) the metal to hydrogen bonding oxygen distances, *V* is the Wigner–Seitz cell volume, θ the water molecule tilt angle of the host lattice, *E* the mean origin energy, Δ the origin splitting, and $\nu_3$ is $\nu_3[Cr(H_2O)_6]^{3+}$. Host lattice data taken from refs. 1–3.

| | *a*/Å | M–O(a)/Å | M–O(2)/Å | *V*/Å$^3$ | θ/° | *E*/cm$^{-1}$ | Δ/cm$^{-1}$ |
|---|---|---|---|---|---|---|---|
| α Alums | | | | | | | |
| $CsAl(SeO_4)_2{\cdot}12H_2$ | 12.544 | 4.063 | 4.091 | 35.5 | 15 | 14 940 | 3.5 |
| $CsGa(SeO_4)_2{\cdot}12H_2O$* | — | — | — | — | — | 14 943 | 3.5 |
| $CsCr(SeO_4)_2{\cdot}12H_2O$ | 12.575 | 4.126 | 4.117 | 37.5 | 18 | 14 943 | 3.5 |
| $CsRh(SeO_4)_2{\cdot}12H_2O$ | 12.532 | 4.131 | 4.080 | 37.5 | 28 | 14 948 | 0.6 |
| $CsIn(SeO_4)_2{\cdot}12H_2O$ | 12.694 | 4.257 | 4.192 | 42.9 | 22 | 14 941 | 7.8 |
| $CsCo(SO_4)_2{\cdot}12H_2O$ | 12.292 | 4.034 | 4.020 | 34.2 | 26 | 14 965 | 9.6 |
| $CsRh(SO_4)_2{\cdot}12H_2O$ | 12.357 | 4.095 | 4.071 | 36.9 | 29 | 14 968 | 5.7 |
| $CsIr(SO_4)_2{\cdot}12H_2O$ | 12.395 | 4.111 | 4.107 | 38.0 | 29 | 14 966 | 3.7 |
| β Alums | | | | | | | |
| $CsAl(SO_4)_2{\cdot}12H_2O$ | 12.357 | 4.069 | 4.050 | 35.7 | 0 | 14 547 | 127 |
| $CsGa(SO_4)_2{\cdot}12H_2O$ | 12.419 | 4.112 | 4.086 | 37.7 | 0 | 14 544 | 128 |
| $CsCr(SO_4)_2{\cdot}12H_2O$ | 12.413 | 4.117 | 4.089 | 37.7 | 0 | 14 543 | 126 |
| $CsIn(SO_4)_2{\cdot}12H_2O$ | 12.540 | 4.230 | 4.161 | 42.7 | 0 | 14 538 | 129 |

* No data available.

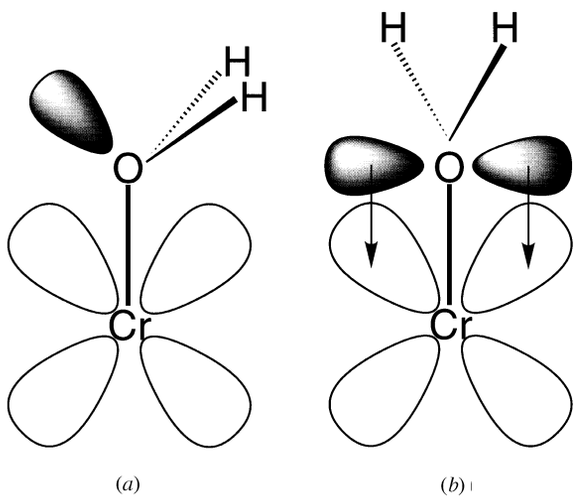


(*a*) (*b*)

**Fig. 5** π-Overlap geometry between the water oxygen lone pair and chromium $t_{2g}$ orbitals: (*a*) trigonal-pyramidal co-ordination in the α alums, (*b*) trigonal-planar co-ordination in the β case

spin–orbit coupling between the $^2E$ and $^2T_2$ states in the presence of a trigonal field.[26] The $^2E$ state splits into two Kramers doublets $2\bar{A}$ and $\bar{E}$, while the splitting of the $^4A_2$ ground state is typically small and only 0.13 cm$^{-1}$ in $CsCr(SO_4)_2{\cdot}12H_2O$.[27]

The magnitude of the $^2E$-state splitting for the α and β alums is determined by the strength of the trigonal field conveyed to the metal $t_{2g}$ orbitals. The trigonal field derives from both the chromium–water π interaction, and the counter-ion polarisation of the chromium orbitals. Variations in the splitting within a class are the result of distortions of the chromium co-ordination environment imposed by the host lattice.

In the β alums, the trigonal-planar water co-ordination results in the oxygen lone pair residing in a p-like orbital normal to the plane of the water molecule (Fig. 5). This configuration geometrically allows π overlap between the lone pair and chromium $t_{2g}$ orbitals. This is confirmed by a recent polarised neutron diffraction study of $CsMo(SO_4)_2{\cdot}12D_2O$ which indicates the presence of highly anisotropic metal–water π bonding normal to the plane of the $sp^2$-hybridised water molecules.[28] The π bonding leads to an angular overlap model which has been used to describe preferential angles of twist in hexaaqua cations.[5] This model defines the splitting of the $t_{2g}$ orbitals into $a_g$ and $e_g$ components as $\delta = |3e_\pi \sin 2\varphi|$, where φ is the twist angle or trigonality and $e_\pi$ is a metal–ligand π-interaction parameter. Maximum π overlap occurs for zero twist but in this case there is zero trigonal component ($T_h$ site symmetry), whereas maximum trigonality minimises π overlap with a twist of −45° (all-horizontal $D_{3d}$ site symmetry). The electronic stabilisation predicted by this model has been used to explain the all-vertical $D_{3d}$ symmetry of $[V(H_2O)_6]^{3+}$, the all-horizontal $D_{3d}$ symmetry of $[Ti(H_2O)_6]^{3+}$, and the failure of vanadium to form α alums with smaller univalent cations.[5,28] Neutron diffraction data for $CsCr(SO_4)_2{\cdot}12H_2O$[5] give a twist angle of −19.0°, and for $CsFe(SO_4)_2{\cdot}12H_2O$[4] of −19.4°. There is no preferential electronic orientation for the $(t_{2g})^3$ electronic configuration of chromium(III). In the ruthenium and vanadium alums where an angle of −45° is electronically favoured a twist angle of only −22° is observed.[5] This illustrates the structure-determining role and strength of the hydrogen bonding in the alum lattice. The origin splitting of the β alums is close to 125 cm$^{-1}$ and almost constant for a variety of host lattices. This large splitting is thus attributed to favourable π overlap geometry, and the constant value for each host lattice to the approximately constant twist angle observed in the β structure.

For α alums the trigonal-pyramidal co-ordination directs the oxygen lone pair away from the metal orbitals. As the angle of tilt is increased from planar towards tetrahedral the character of the oxygen lone-pair orbital will vary from p to $sp^3$ with decreasing π overlap. The extent of π overlap with the metal ion also effects the mean electronic origin energy. The transition is intra $t_{2g}$ with a spin-pairing component, and variations in the transition energy are a consequence of a π-bonding nephelauxetic effect. The difference in α and β origin energies is attributed to larger π overlap in the β alums and is consistent with a larger trigonal field.

The angle of tilt in the α host lattices (θ) cannot be determined directly due to the absence of neutron diffraction data and the large errors associated with hydrogen positions in X-ray results. The co-ordinated water molecule is considered to adopt a tilt angle similar to that of the host lattice to maintain hydrogen-bond linearity. The tilt angle shown in Table 1 is calculated approximately by assuming hydrogen-bond linearity, and considering the plane defined by the metal water oxygen O(b) and the oxygens of the caesium cation O(a) and sulfate anion O(2) involved in the hydrogen bonding. The difference in $Cr{-}OH_2$ and $M{-}OH_2$ bond lengths has a negligible effect in determining the expected tilt. The tilt angle is largest for the sulfate α alums, minimising π interaction with the $(t_{2g})^6$ metal orbitals. These alums, however, generally exhibit larger origin splittings than those of the selenate alums. The origin splitting for the sulfate α alums is instead attributed to the trigonal polarisation and deformation of the oxygen charge cloud by hydrogen bonding to groups trigonally oriented along the

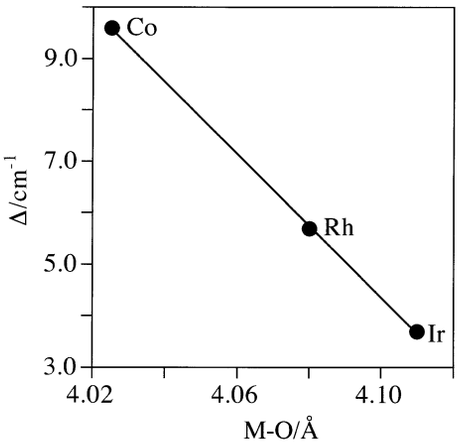


**Fig. 6** Relationship between origin splitting and chromium site size, indicated by the average of M–O(a) and M-O(2), in the sulfate α alums

three-fold axis. This results in a small trigonal polarisation of the metal orbitals. A similar polarisation argument was used to explain the splitting of chromium(III) in emerald where the $CrO_6$ octahedron is almost regular.[29] The stronger hydrogen bonding and polarising strength of sulfate over selenate is illustrated in the splittings of the rhodium alums. For an almost identical angle of tilt the splitting in the sulfate alum is over 10 times larger than that in the selenate. The decrease in splitting in the series cobalt, rhodium, iridium is linear with increasing chromium site size (Fig. 6), and is attributed to the corresponding decrease in polarisation strength. The electronic origin energies are approximately constant for these α alums reflecting no change in covalency as expected for minimum π overlap.

For the selenate alums the polarisation effect is smaller and the splittings are predominantly attributed to π overlap. The π overlap is larger for most of the selenate alums than for the sulfate α alums, due to the reduced angle of tilt. This is reflected in the lower α-alum origin energy for the selenate alums. The tilt in the aluminium alum is 3° less than that for chromium, producing a slightly lower origin energy. The same splitting is observed in each case indicating that the trigonal field is comparatively less sensitive to changes in the tilt angle. This is a result of the opposing effects of trigonal geometry and π overlap on the total trigonal field strength. While the geometrical component of the trigonal field is enhanced with increased tilt angle, the magnitude of the field at chromium is decreased due to the concomitant decrease in π overlap. There is no crystal structure available for the gallium alum, however it is expected to be similar to that of the chromium alum since the ionic radii are almost identical. There is no difference in splitting or origin energy for the two alums. In the rhodium selenate case the large angle of tilt results in almost no splitting and the highest origin energy of the selenates. The splitting for the indium alum is larger than expected for the host lattice tilt angle. It is possible that the large size of the chromium site in this lattice results in a co-ordination environment no longer tightly constrained by the hydrogen bonding, allowing distortion towards the more usual trigonal-planar co-ordination.

## Conclusion

The larger origin splitting and lower origin energy for the β series, compared with the α alums, is attributed to larger π overlap associated with water co-ordination geometry. In the selenate alums the tilt angle of the co-ordinated water molecule increases with increasing site size, reducing the π overlap, decreasing the splitting, and increasing the origin energy. This trend breaks down for the very large indium selenate site. In the sulfate α alums the large angle of tilt due to the $(t_{2g})^6$ configuration of the host lattice results in little π overlap and is reflected in the uniformly high transition energies. The splitting is instead attributed to polarisation by the trigonally oriented sulfate groups, the effect of which decreases with increasing site size. Vibrational energies also decrease with site size.

This work indicates that dilution by isomorphous substitution into an appropriate lattice results in subtle variations in the dopant co-ordination sphere. The dopant distorts to meet the requirements of the host-lattice, in this case imposed by hydrogen bonding. The magnitude of the variations are largely dependent upon the host lattice site size compared with that of the pure dopant. For similar site sizes, such as in the gallium alum, there is effectively no distortion. Large variations are seen, however, for the rhodium and indium alums, or when the chromium occupies a sulfate lattice with the α form. It is only possible to probe these site-size effects due to the sensitivity of the luminescence experiment.

## Acknowledgements

We thank Dr. S. P. Best for helpful discussions, Dr. D. R. Brown for assistance with the figures, Dr. G. J. Long for supplying the Wigner–Seitz program BLOKJE, and the Australian Research Council for financial support.

## References

1 J. K. Beattie, S. P. Best, B. W. Skelton and A. H. White, *J. Chem. Soc., Dalton Trans.*, 1981, 2105.
2 R. S. Armstrong, J. K. Beattie, S. P. Best, G. P. Braithwaite, P. Del Favero, B. W. Skelton and A. H. White, *Aust. J. Chem.*, 1990, **43**, 393.
3 R. S. Armstrong, J. K. Beattie, S. P. Best, B. W. Skelton and A. H. White, *J. Chem. Soc., Dalton Trans.*, 1983, 1973.
4 S. P. Best and J. B. Forsyth, *J. Chem. Soc., Dalton Trans.*, 1990, 395.
5 S. P. Best and J. B. Forsyth, *J. Chem. Soc., Dalton Trans.*, 1991, 1721.
6 S. P. Best and J. B. Forsyth, *J. Chem. Soc., Dalton Trans.*, 1990, 3507.
7 G. J. Goldsmith, F. V. Shallcross and D. S. McClure, *J. Mol. Spectrosc.*, 1965, **16**, 296.
8 R. L. Carlin and I. M. Walker, *J. Chem. Phys.*, 1967, **46**, 3921.
9 F. D. Camassei and L. S. Forster, *J. Mol. Spectrosc.*, 1969, **31**, 129.
10 C. D. Flint and P. Greenough, *J. Chem. Soc., Faraday Trans. 2*, 1972, 897.
11 C. D. Flint, P. Greenough and A. P. Matthews, *J. Chem. Soc., Faraday Trans. 2*, 1973, 23.
12 C. D. Flint and P. Greenough, *J. Chem. Soc., Faraday Trans. 2*, 1974, 815.
13 C. D. Flint and A. P. Matthews, *J. Chem. Soc., Faraday Trans. 2*, 1974, 1301.
14 P. Greenough and A. G. Paulusz, *J. Chem. Phys.*, 1979, **70**, 1967.
15 D. L. Kraus and G. C. Nutting, *J. Chem. Phys.*, 1941, **9**, 133.
16 L. Grabner, R. A. Forman and E. Y. Wong, *Phys. Rev. B*, 1972, **6**, 797.
17 R. S. Armstrong, S. P. Best, B. D. Cole and K. W. Nugent, *Proceedings of the Twelth International Conference on Raman Spectroscopy*, eds. J. R. Durig and J. F. Sullivan, Wiley, New York, 1990, p. 414.
18 D. A. Johnson and A. G. Sharpe, *J. Chem. Soc. A*, 1966, 798.
19 S. P. Best, R. S. Armstrong and J. K. Beattie, *J. Chem. Soc., Dalton Trans.*, 1982, 1655.
20 S. P. Best, R. S. Armstrong and J. K. Beattie, *Inorg. Chem.*, 1980, **19**, 1958.
21 S. P. Best, J. K. Beattie, R. S. Armstrong and G. P. Braithwaite, *J. Chem. Soc., Dalton Trans.*, 1989, 1771.
22 S. P. Best, J. K. Beattie and R. S. Armstrong, *J. Chem. Soc., Dalton Trans.*, 1984, 2611.
23 R. S. Armstrong, J. K. Beattie, S. P. Best, B. D. Cole and P. L. W. Tregenna-Piggott, *J. Raman Spectrosc.*, 1995, **26**, 921.
24 L. Gelato, *J. Appl. Crystallogr.*, 1981, **14**, 151.
25 S. Sugano and Y. Tanabe, *J. Phys. Soc. Jpn.*, 1958, **13**, 880.
26 S. Sugano and I. Tsujikawa, *J. Phys. Soc. Jpn.*, 1958, **13**, 899.
27 B. Bleaney, *Proc. R. Soc. London, Ser. A*, 1950, **204**, 203.
28 S. P. Best, B. N. Figgis, J. B. Forsyth, P. A. Reynolds and P. L. W. Tregenna-Piggott, *Inorg. Chem.*, 1995, **34**, 4605.
29 J. L. Wood, *J. Chem. Phys.*, 1965, **42**, 3404.

*Received* 14*th August* 1996; *Paper* 6/05705E